Applied Microbiology and Biotechnology (2022) 106:2017–2027
https://doi.org/10.1007/s00253-022-11823-3

BIOTECHNOLOGICALLY RELEVANT ENZYMES AND PROTEINS

High-temperature behavior of hyperthermostable *Thermotoga maritima* xylanase XYN10B after designed and evolved mutations

Yawei Wang[1] · Jing Wang[2] · Zhongqiang Zhang[2] · Jiangke Yang[1] · Ossi Turunen[3] · Hairong Xiong[2]

Received: 12 November 2021 / Revised: 29 January 2022 / Accepted: 5 February 2022 / Published online: 16 February 2022

Abstract

A hyperthermostable xylanase XYN10B from *Thermotoga maritima* (PDB code 1VBR, GenBank accession number KR078269) was subjected to site-directed and error-prone PCR mutagenesis. From the selected five mutants, the two site-directed mutants (F806H and F806V) showed a 3.3–3.5-fold improved enzyme half-life at 100 °C. The mutant XYNA generated by error-prone PCR showed slightly improved stability at 100 °C and a lower K_m. In XYNB and XYNC, the additional mutations over XYNA decreased the thermostability and temperature optimum, while elevating the K_m. In XYNC, two large side-chains were introduced into the protein's interior. Micro-differential scanning calorimetry (DSC) showed that the melting temperature (T_m) dropped in XYNB and XYNC from 104.9 °C to 93.7 °C and 78.6 °C, respectively. The detrimental mutations showed that extremely thermostable enzymes can tolerate quite radical mutations in the protein's interior and still retain high thermostability. The analysis of mutations (F806H and F806V) in a hydrophobic area lining the substrate-binding region indicated that active site hydrophobicity is important for high activity at extreme temperatures. Although polar His at 806 provided higher stability, the hydrophobic Phe at 806 provided higher activity than His. This study generates an understanding of how extreme thermostability and high activity are formed in GH10 xylanases.

Key points

- *Characterization and molecular dynamics simulations of TmXYN10B and its mutants*
- *Explanation of structural stability of GH10 xylanase*

Keywords Thermostability · GH10 xylanase · Mutation · 1VBR · *Thermotoga maritima*

Introduction

Endo-1,4-β-D-xylanases (E.C.3.2.1.8) catalyze the hydrolysis of 1,4-β-D-xylosidic linkages in xylan. They are widespread enzymes, involved in the production of xylose, a primary carbon source for cell metabolism. Hemicellulase is a general term used to describe a cocktail of hydrolytic enzymes used to depolymerize plant hemicelluloses (Dumon et al. 2008). Endo-xylanase, one of the main hemicellulases, randomly hydrolyzes the β-1,4-glycosidic bonds of xylan to produce xylo-oligosaccharides and xylose. Xylanase enzymes have immense potential in various industrial applications that include biomass hydrolysis or modification (Collins et al. 2005; Chaudhary et al. 2021).

Thermostable xylanases are widely used in biotechnological processes operated at high temperatures (Basit et al. 2018). Application of thermostable enzymes in industrial processes that are carried out at high temperatures has several advantages (Hämäläinen et al. 2016; Kumar et al. 2018). Furthermore, thermostable enzymes are promising to be used together with ionic liquids in biomass treatments (Hebal et al. 2020, 2021). An area of intensive industrial application for xylanases has been the deconstruction of plant cell-wall components to facilitate pulp bleaching and

✉ Ossi Turunen
ossi.turunen@uef.fi

✉ Hairong Xiong
xionghr@mail.scuec.edu.cn

[1] College of Life Science and Technology, Wuhan Polytechnic University, Wuhan 430048, China

[2] College of Life Science, South-central University for Nationalities, Wuhan 430074, China

[3] School of Forest Sciences, University of Eastern Finland, FI-80101 Joensuu, Finland

biofuel production from lignocellulose (Taylor et al. 2009; Bhalla et al. 2013; Chaudhary et al. 2021).

Rational design and directed evolution methods have widely been used to improve the properties of xylanases for meeting the requirement of industrial applications (Wang et al. 2012; Li et al. 2013; Wang et al. 2014; Torktaz et al. 2018; Yang et al. 2020; Lai et al. 2021; Li et al. 2021; Yi et al. 2021). In addition, a major goal in the enzyme engineering research is to improve the understanding of structure–function relationships. Unlike rational design, random mutation methods such as error-prone PCR do not require an extensive knowledge of protein structure and the dependence of stability properties on structural features. Thus, random mutation has been widely applied to improve xylanase thermostability, activity, and alkalophilicity (Miyazaki et al. 2006; Dumon et al. 2008; You et al. 2010; Song et al. 2015).

A hyperthermostable GH10 xylanase XYN10B from *Thermotoga maritima* (herein named TmXYN10B) (Winterhalter and Liebl 1995; Ihsanawati et al. 2005; Yu et al. 2016; Yang and Han 2018) having its apparent temperature optimum at 100 °C in 30-min assay (Yu et al. 2016) was investigated in this study. Site-directed and error-prone mutagenesis, as well as structural analysis, was used to generate new understanding of the functioning of this enzyme.

Materials and methods

Strains, vectors, and materials

Escherichia coli BL21 (DE3) cells (Transgen, Beijing, China) were used as the host for prokaryotic protein expression and were grown aerobically in Luria–Bertani broth with 100 μg ampicillin/mL. All enzymes were purchased from Takara Bio (Shiga, Japan). Beechwood xylan, used as the substrate in the xylanase assay, was purchased from Sigma-Aldrich (X4252, St. Louis, MO, USA). Cloning primers were synthesized by Tsingke Biotech (Wuhan, China). All chemical reagents were analytical grade.

Construction of the recombinant plasmid

The extremely thermostable xylanase gene *xynh* sequence of TmXYN10B was codon-optimized for expression in *E. coli*. The full-length xylanase gene *xynh* was synthesized by Tsingke Biotech. The mature gene without an intron was inserted between the cleavage sites *Xho*I and *Nco*I of plasmid pET-22b(+) (Takara Bio, Shiga, Japan). When the gene was inserted into pET-22b(+), the termination codon was removed to link the polyhistidine tag to the C-terminal side of the xylanase protein.

Site directed mutagenesis of TmXYN10B

Swiss-PdbViewer (https://spdbv.unil.ch/) was used to design the site-directed active site mutations of TmXYN10B. The mutations were generated using PCR primers containing the mutated codons as described earlier (Wang et al. 2012). When the position of the mutation was in the middle of the xylanase gene, overlap-extension PCR was used to introduce the mutations (Wang et al. 2012).

Random mutagenesis of TmXYN10B by error-prone PCR

Random mutagenesis by error-prone PCR (Miyazaki et al. 2006) was conducted using a modified PCR system (1.5 μL of *Taq* polymerase, 5 μL of *Taq* polymerase buffer, 2 μL of forward primer (5'–CGCCATGGATTCTCAGAA TGTATC–3'), 2 μL of reverse primer (5'–TCGCGACTC GAGTTTTCTTTCTTC–3'), 2 μL of templates, 5 μL of 8 mM Mn^{2+}, 5 μL of 25 mM Mg^{2+}, 4 μL of 5 mM dTTP, 4 μL of 5 mM dCTP, 4 μL of 2.5 mM dNTPs, and 15.5 μL of H_2O). The DNA sequence encoding the mature protein of TmXYN10B was used as a template. The PCR reaction was conducted as follows: 95 °C for 5 min followed by 35 cycles of 95 °C for 30 s, 52 °C for 35 s and 72 °C for 1 min, and a final 5 min extension at 72 °C. The products were double-digested by *Xho*I and *Nco*I and then ligated with similarly digested vector pET-22b(+). The ligation mixture was transformed into *E. coli* TOP10 (Tsingke, Wuhan, China) by heat-shock treatment. After three rounds of sequential error-prone PCR, non-specific amplification occurred, and then the final PCR products were purified, ligated with linearized pET-22b(+), and transformed into *E. coli* BL21(DE3) for the expression of the mutants.

Expression of the mutants in E. coli

The constructed plasmid pET-22b(+)-TmXYN10B was transformed into *E. coli* BL21 (DE3) competent cells. The cells were cultivated at 37°C for 12 h, and then, the protein expression was induced by isopropyl-β-D-thiogalactopyranoside (IPTG) at a final concentration of 0.5 mM and incubated at 28 °C for 16 h (Yu et al. 2016). All mutations were confirmed by sequencing.

Purification of proteins

The culture supernatant of the recombinant *E. coli* BL21 (DE3) was collected by centrifugation at 10,000× *g* in 4 °C for 15 min. The cell-free supernatant was filtered using a 10 kDa membrane. The filtered supernatant was loaded

into a 1 mL immobilized Ni^{2+} affinity column (Novagen, Madison, WI, USA) and eluted with elution buffer (0.4 M imidazole, 0.5 M NaCl, and 20 mM Tris-HCl, pH 7.9). The eluent was concentrated and analyzed by sodium dodecyl sulfate polyacrylamide gel electrophoresis (SDS-PAGE) 12% (wt/vol) gel. The protein bands were analyzed by density scanning using an image analysis system. The protein concentrations were determined by the Bradford method using bovine serum albumin (BSA) as the standard (Yu et al. 2016; Wang et al. 2020). The protein concentration of enzymes was adjusted at 4 mg/ml, and the purified enzymes were diluted for the specific activity assays.

Enzymatic activity assays

The enzymatic activity of xylanases was determined by reaction in 1 mL mixture containing 100 µL of appropriately diluted enzymes and 900 µL of 0.5% (*w/v*) beechwood xylan, which was dissolved in 50 mM phosphate buffer, pH 5.0. The 3, 5-dinitrosalicylic acid (DNS) method with a 10 min assay was used for determination of the enzyme activity (Wang et al. 2012). One unit of xylanase enzyme activity (IU) was defined as 1 µmol of D-xylose released per minute.

The temperature optima were determined by incubating the enzymes and substrates in 50 mM phosphate buffer at pH 5 for 10 min, at intervals of 10 °C from 60 °C to 100 °C. The optimal pH of xylanases was measured at the optimal temperature of enzymes for 10 min from pH 4.0 to 8.0, and the buffer was 50 mM citric acid buffer in the pH range of 4.0 to 7.0, as well 50 mM Tris-HCl buffer at pH 8.0.

The time-dependent decrease in enzyme activity was used for the calculation of enzyme half-life (Wang et al. 2012). After incubations of up to 120 min at 100 °C and pH 5.5, the residual activity was measured at 90 °C, pH 5.5. The half-life time was calculated from the decreasing of the reaction product as a function of time. The Arrhenius activation energy (E_a) was calculated with the Arrhenius Equation (Turunen et al. 2004). All experiments were performed in triplicates.

Differential scanning calorimetry

Differential scanning calorimetry (DSC) was used to analyze the thermodynamic stability (T_m) of TmXYN10B and its mutants (Chawachart et al. 2014; Tu et al. 2015). A Nano-DSC (TA Instruments, New Castle, DE, USA) was run at a heating and scanning rate of 1 °C/min over a temperature range of 50 to 110 °C, with an enzyme concentration of 4 mg/mL in 50 mM citrate phosphate buffer at pH 5.5.

Differential scanning fluorimetry

Differential scanning fluorimetry (DSF) was used to determine the apparent melting temperature (T_m^{app}) values for mutants (Ericsson et al. 2006; Bommarius and Paye 2013; Johnson et al. 2014; Li et al. 2018). The T_m^{app} was defined as the maximal value of the relative fluorescence change with respect to the temperature (dRFU/dT). For each analyzed sample, 5 µL of 100×SYPRO Orange solution (Life Technologies, Carlsbad, CA, USA) and 20 µL of purified protein were mixed and then centrifuged for 5 min at 4 °C. The T_m^{app} was determined by heating the samples from 50 to 99 °C at 1 °C/min in a StepOnePlus real-time PCR system (Life Technologies, Carlsbad, CA, USA).

Molecular dynamics simulations

The TmXYN10B structure was used with xylotetraose docked by SwissDock (http://www.swissdock.ch/docking) into the active site (docking described by Hebal et al. 2020) to perform the molecular dynamics simulations for the wild-type TmXYN10B and the mutants XYNH and XYNV. The binding free energies were calculated using the MM-PBSA method for xylotetraose in the active site (Tu et al. 2018).

Results

Sequence information of TmXYN10B and its mutants

The codon-optimized TmXYN10B gene (GenBank accession number KR078269) was prepared by gene synthesis.

Table 1 *Thermotoga maritima* xylanase TmXYN10B mutants. Common mutations among XYNA, XYNB, and XYNC were underlined

Mutant	GenBank accession number	Mutations
XYNA	OL444891	D592G, V632A, K789E, I837M
XYNB	OL444892	N562D, T568M, R575G, D592G, V632A, D643G, K789E, Q792L, I837M
XYNC	OL444893	N536I, M564K, D592G, V632A, K789E, L833W, I837M
XYNH	OL444894	F806H
XYNV	OL444895	F806V
TmXYN10B	KR078269	

The amino-acid numbering followed the numbering in PDB structure 1VBR. Accordingly, the catalytic acid/base is E647 and the nucleophile is E753. The mutations and amino-acid sequences of TmXYN10B and its mutants are shown in Table 1 and Supplemental Fig. S1, respectively. While the theoretical molecular weight of TmXYN10B is 38.6 kDa, TmXYN10B and its mutants showed a protein band between the 35 kDa and 45 kDa molecular weight markers (~42 kDa), as determined by SDS-PAGE analysis (Supplemental Fig. S2), a size that is in line with the expressed 328 amino acids of the protein.

The site-directed mutants XYNH (F806H, GenBank accession number OL444894) and XYNV (F806V, GenBank accession number OL444895), as well as several error-prone PCR mutants, were investigated in this study. A total of 121 active mutant colonies were verified after the error-prone PCR. Among these 121 mutants, XYNA (D592G, V632A, K789E, and I837M, GenBank accession number OL444891), XYNB (N562D, T568M, R575G, D592G, V632A, D643G, K789E, Q792L, and I837M, GenBank accession number OL444892), and XYNC (N536I, M564K, D592G, V632A, K789E, L833W, and I837M, GenBank accession number OL444893) were selected for characterization (Table 2). XYNA was the starting enzyme for XYNB and XYNC; thus, it contained several common mutations (Table 1).

Effect of mutations on thermal activity and stability

The graphs of temperature-dependent activity showed that the optimum temperature for the activity of TmXYN10B, XYNA, XYNH, and XYNV could be higher than 100 °C (Fig. 1). However, the random mutants XYNB and XYNC showed the highest activity at 90 °C and 70 °C, respectively.

The mutations at the edge of the active-site canyon (F806H in XYNH and F806V in XYNV) significantly elevated the stability at 100 °C since the half-life increased over 3-fold, and in addition, the melting temperature (T_m) increased slightly (Table 2). This shows that the extremely thermostable TmXYN10B still has potential in its structure to become further stabilized. However, the increase in stability was followed by lowered specific activity (Table 2) and catalytic performance, as expressed by the V_{max}/K_m ratio (Table 2). This indicates that the stability of this hyperthermostable enzyme is already at such a high level that increasing it further may compromise the activity values. Although the mutants XYNH and XYNV showed lower specific activities as in Table 2, when the increase of thermostability is the main goal, some decrease of activity could be tolerated.

The thermostability graphs for calculation of the half-life of TmXYN10B and its mutants were shown in Fig. 2. The random mutant XYNA showed an improved half-life at 100 °C, but its stability was decreased at temperatures over 100

Table 2 Summary of properties of TmXYN10B and its mutants

	Optimum temperature (°C, 10-min assay)	T_m by DSC (°C)	T_m^{app} by DSF (°C)	Half-life at 100 °C (min)	Optimum pH (10min)	Specific activity[a] (Umg^{-1}, 90°C)	Specific activity[a] (Umg^{-1}, 70°C)	K_m ($mgml^{-1}$,70°C) [a]	V_{max} (mmol min^{-1} mg^{-1})	V_{max}/K_m	E_a (kJ mol^{-1})
TmXYN10B	˃100	104.9	˃100	110	5.5	10597±477	2177±167	0.51±0.02	1.928±0.012	3.78	75.68[b]
XYNH	˃100	105.8	˃100	391	5.5	7384±135	620±42	0.45±0.04	0.589±0.007	1.31	44.99[b]
XYNV	˃100	105.3	˃100	368	5.5	7218±143	552±13	0.56±0.02	1.406±0.002	2.51	74.37[b]
XYNA	˃100	101.7	97.6	185	5.5	10633±382	2092±155	0.33±0.04	1.632±0.023	4.95	62.77[b]
XYNB	90	93.7	87.9	6.8	5.5	1377±69	984±65	9.18±0.66	0.682±0.046	0.07	20.82[c]
XYNC	70	78.6	73.5	3.6	5.5-6.0	643±55	1362±94	9.65±0.34	0.751±0.024	0.08	45.57[d]

[a]Results based on 3 biological replicates (± sd); [b]results by 50-100°C; [c]result by 40-90°C; [d]Result by 40-70°C.

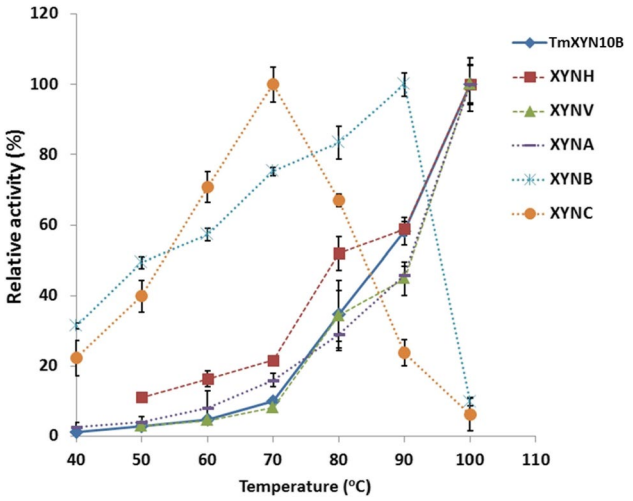

Fig. 1 Effect of temperature on the activities of TmXYN10B and its mutants. The maximal activity in each curve was defined as 100%

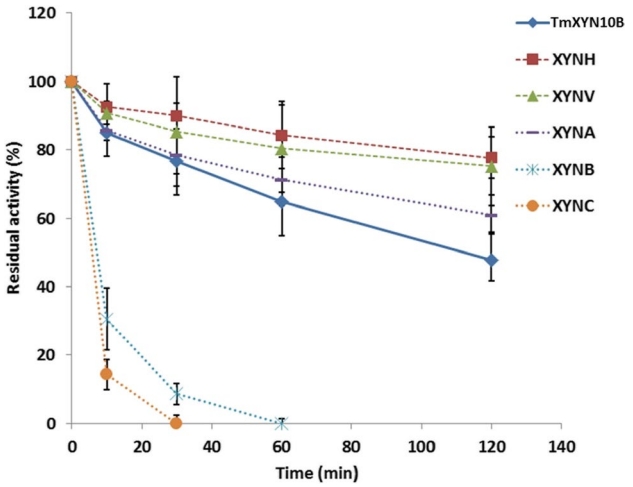

Fig. 2 Thermostability of TmXYN10B and its mutants. After 120 min incubation at 100 °C and pH 5.5, the residual activities were measured at 90 °C, pH 5.5

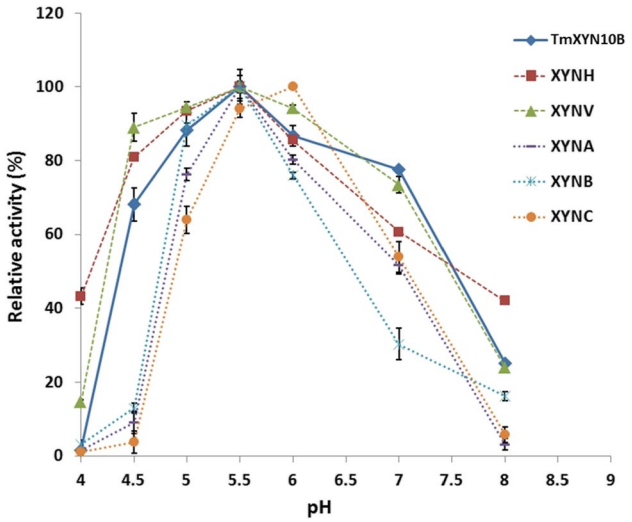

Fig. 3 pH-dependent activities of TmXYN10B and its mutants. TmXYN10B, XYNH, XYNV, and XYNA were measured at 90 °C, whereas XYNB and XYNC were measured at 70 °C

°C (T_m decreased slightly). A reason for this XYNA behavior, which at first glance looks conflicting, could be that there are reversible conformational changes that return to normal conformation allowing the enzyme activity after incubation at high temperature when the temperature is lowered to measuring the activity at 70 °C. Instead, in measuring the T_m at around 100 °C, the possible reversible conformational changes are on and affect the T_m value. Therefore, T_m showed decreased stability at around 100 °C, and half-life at 100 °C showed increased stability for XYNA. The K_m of XYNA decreased slightly, thereby improving V_{max}/K_m, but this was not reflected in its specific activity, which remained at the wild-type level (Table 2). This indicated that theoretical kinetic values may not always reflect accurately the activity in standard measuring conditions.

XYNB and XYNC showed a dramatic drop in the temperature optimum showing that some or all of the mutations were destabilizing. The pH optimum region was not much different between XYNA, XYNB, XYNH, and XYNV having the optimum at pH 5.5, whereas XYNC exhibited a higher activity at pH 6.0 (Fig. 3). However, XYNA, XYNB, and XYNC had much narrower pH profiles than the wild type or XYNH and XYNV. The consequence was a relatively low xylanase activity at pH 4.5 (Fig. 3). Therefore, in addition to lowered thermostability, the mutations in XYNA, XYNB, and XYNC decreased their tolerance to acidic and alkaline conditions.

DSC and DSF analyses

DSC was performed to determine the T_m values of the wild type TmXYN10B and its mutants over a temperature range of 50 to 110 °C. In comparison with the T_m of TmXYN10B (104.9 °C), the T_m values of the XYNH and XYNV mutants showed increases of 0.9 °C (105.8 °C) and 0.4 °C (105.3 °C), respectively. However, the XYNA, XYNB, and XYNC mutants exhibited lower T_m values of 101.7 °C, 93.7 °C, and 78.6 °C, respectively (Table 2, Fig. 4).

DSF has been used to determine the thermostability of xylanase in other reports (Katewadee et al. 2021). In this study, DSF was used to determine the thermostability of TmXYN10B and its mutants using a purified enzyme. The T_m^{app} values of the mutants XYNA,

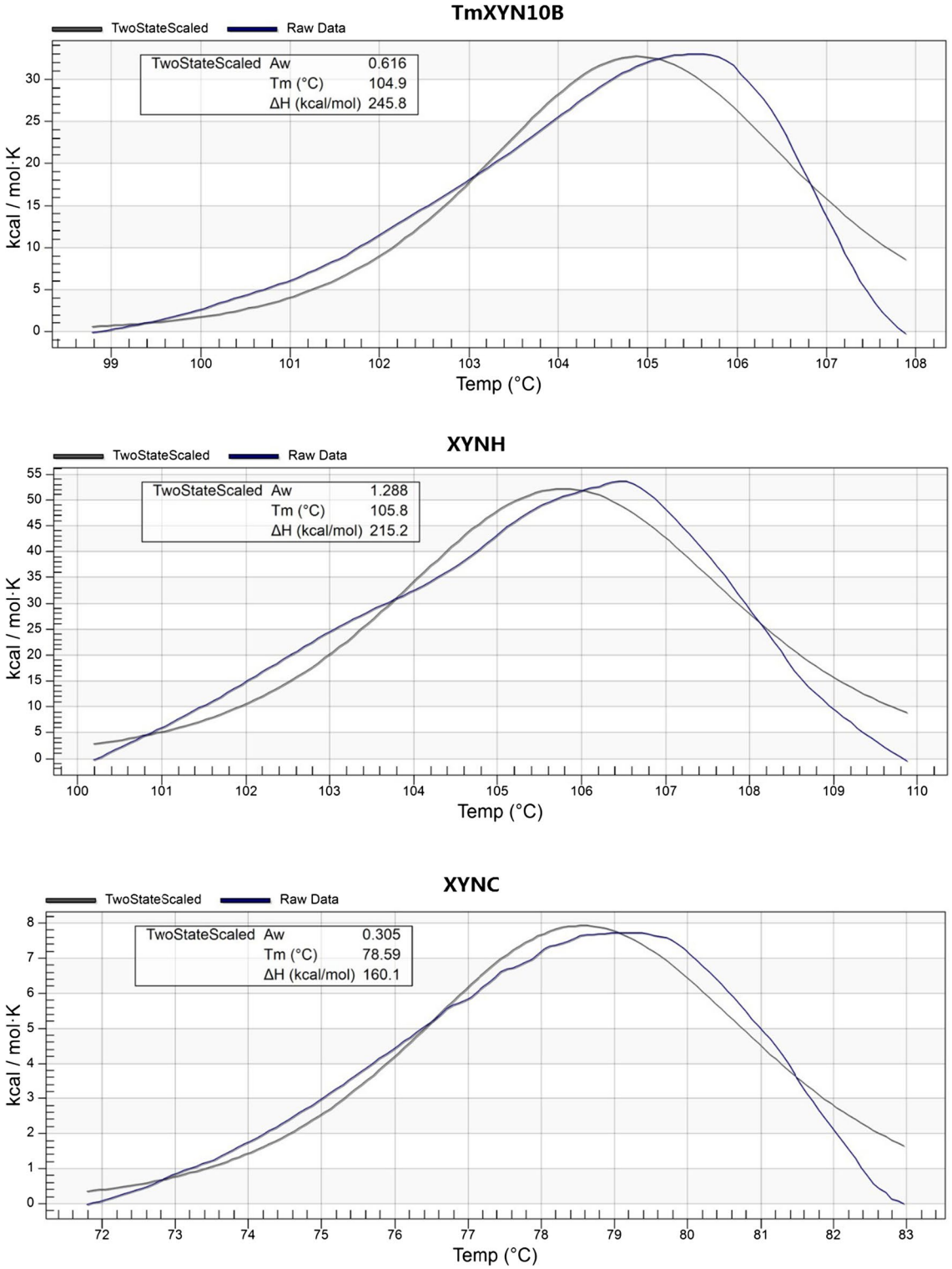

Fig. 4 Differential scanning calorimetry (DSC) results

XYNB, and XYNC were 97.6 °C, 87.9 °C, and 73.5 °C, respectively, which were lower than that of TmXYN10B. The apparent melting temperatures measured for these variants by DSF were each lower by about 5 °C and relatively corresponded with the values obtained by DSC (Table 2). On the other hand, the trend curve showed that the T_m^{app} values of TmXYN10B, XYNH, and XYNV may be higher than 99 °C (Fig. 5). Thus,

the DSF values in general supported the stability order results obtained by DSC.

Structural analysis of the mutations

Active-site mutations were designed for TmXYN10B at the position 806 lining the substrate in the wall of the active site (Fig. 6). The mutations at this position in XYNH and XYNV were F806H and F806V, respectively. The His side chain likely formed a hydrogen bond to the substrate (Fig. 6B), and this may have caused a slight decrease in the K_m of XYNH (from 0.51 mg/ml of the wild type to 0.45 mg/ml of XYNH). However, the specific activity (but V_{max} not as much) was similarly lowered after the mutation F806V in XYNV (Table 2). Thus, it seems that many active site mutations are not optimal for the activity and various reasons may explain the effects.

The molecular dynamics simulation with docked xylotetraose showed the lowest delta-G energy for F806H. The wild type with Phe and two mutations (F806V and F806L, the latter not synthesized) showed higher delta-G energies (Table 3). Furthermore, F806H resulted in the highest stability values even without the presence of substrate (according to T_m by DSC and T_{half} at 100 °C). The Arrhenius activation energy was lowered in XYNH (Table 2 and Supplemental Fig. S3), indicating that this mutation potentially also increased structural flexibility, despite significantly increasing stability.

F806 exhibits hydrophobic interactions with the nearby side-chains of W802 and F807 in the TmXYN10B structure (Fig. 6A). The side-chains of these residues form a strong hydrophobic patch lining the active site (Supplemental Fig. S4). The short side-chain of Val also contributed to hydrophobic packing with the side-chains of W802 and F807, which unexpectedly improved the thermostability significantly, but the specific activity was decreased. Val at position 806 had no contact with the substrate (Fig. 6C).

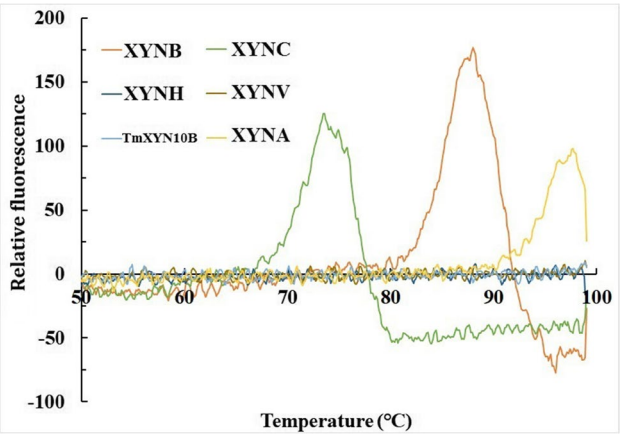

Fig. 5 Differential scanning fluorimetry (DSF) results

Discussion

Aromatic residues have important roles in the enzyme active sites, take part in substrate binding and moving in the active site and determine the substrate specificity, and affect the thermostability of the enzymes (Nakamura et al. 2013; Tian et al. 2016; Kashif et al. 2017; Prajapati et al. 2018). The mutation of active site aromatic residues may affect the stability and activity properties of the active site and the protein flexibility (Kashif et al. 2017). Enzyme activity requires a certain amount of flexibility of the active site and too high stability may compromise the activity (Shoichet et al. 1995; Kamerzell and Middaugh 2008).

The active site of TmXYN10B contains a strong hydrophobic patch (W802, F806, and F807) interacting with approximately four xylose units of the substrate from one side of the active site canyon. The role of this patch was studied by replacing the middle-most side chain F806 to polar His (Fig. 6A), thus, weakening the hydrophobic interaction and introducing a new polar interaction to this region. Also, F806V shifted the center of hydrophobicity at this site away from a contact with the substrate.

The results showed that for this enzyme, the native long hydrophobic side-chain of Phe at position 806 resulted in the highest activity, whereas the equally long polar side-chain of His at position 806 forming a potential H-bond to the substrate resulted in the highest stability. It can be concluded that the hydrophobic interaction between F806 and hydrophobic regions of the substrate is likely optimal for enzyme activity at high temperatures. Hydrophobic effects become stronger at higher temperatures, and hydrophobic interactions appear to dominate in the highly thermophilic proteins (Gromiha et al. 2013; van Dijk et al. 2015; Wu et al. 2020). Hydrogen bonds also play a role, but there are fewer hydrogen bonds at higher temperatures and they are typically weaker (Dougherty 1998; Camilloni et al. 2016). The mutations at position 806 showed that the TmXYN10B active site is at least partly optimized for high activity at extreme temperatures by optimizing hydrophobic interactions.

The active site configurations of the corresponding region in various GH10 xylanases (PDB structures 1us2, 1v6u, 2cnc, 2f8q, 2wys, 3nj3, 3u7b, 3w24, 4hu8, 4l40, 4pmx, 5ay7, 5eff, 5xzo, 6jdt, 6wqw, and 7d88) were also compared in the region corresponding to W802-F806-F807 in TmXYN10B. Great variation exists in this region (not shown). Only *Thermotoga* enzymes have a similar hydrophobic patch than TmXYN10B. A couple of enzymes having a lower thermostability have a hydrophobic band of four hydrophobic residues (W-F-P-F/W in PDB structures 4L4O and 6WQW) lining the substrate-binding site. GH10 xylanase (Uniprot Q9R6T4) from *Thermotoga* sp. strain FjSS3-B.1 strain is one of the most thermostable GH10 xylanases

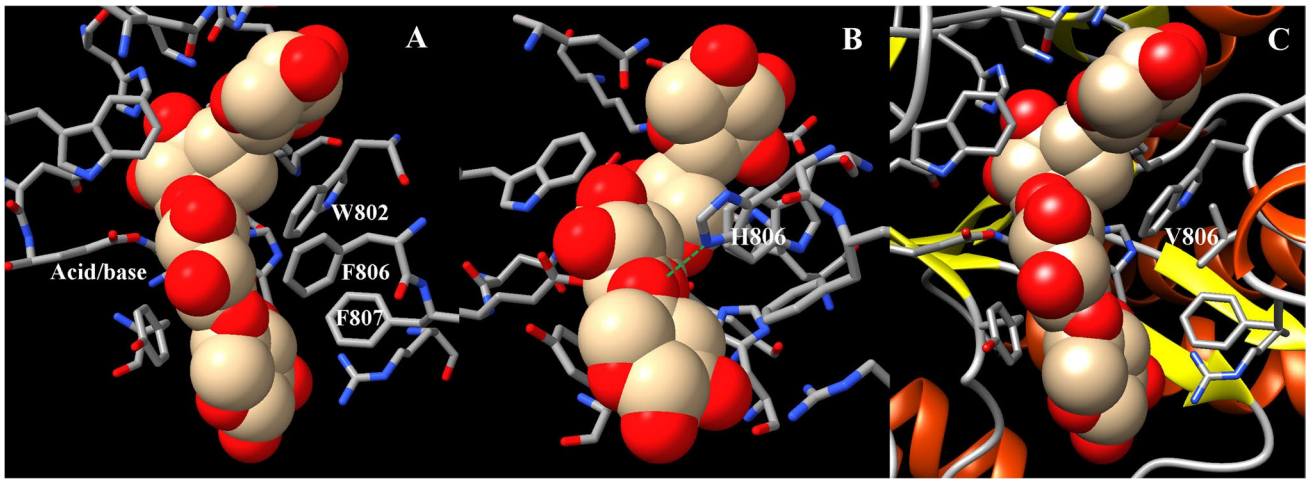

Fig. 6 The active site is shown for the wild type TmXYN10B (A), XYNH with mutation F806H (B), and XYNV with mutation F806V (C). Xylotetraose was docked by SwisDock to the active site (Yu et al. 2016). The green dashed line shows the potential H-bond from F806H to the glycosidic oxygen. Xylotetraose is shown in sphere form indicating the van der Waals volume. The image was prepared with UCSF Chimera (https://www.rbvi.ucsf.edu/chimerax/)

(temperature optimum 105 °C; Simpson et al. 1991). By doing modeling by Swiss-Model (https://swissmodel.expasy.org/; data not shown), the active site region corresponding to W802-F806-F807 in TmXYN10B is completely different in FjSS3-B.1 after the extremely conserved tryptophan. Furthermore, in the FjSS3-B.1 enzyme, this area is quite polar. This comparison shows that different GH10 enzymes having their optimal activity in different temperature regions utilize unique active site structures for substrate binding.

The error-prone PCR mutations also revealed insights how extreme thermostability is formed in TmXYN10B. Spatial structural examination showed that all four mutation sites of XYNA were on the other side of the enzyme on the protein surface when compared to the catalytic center. In contrast, the five additional mutations in XYNB included one mutation (N562D) in the catalytic center and another (T568M) close to it on the protein surface, whereas one was on the protein surface (R575G) and two were in the protein's interior (Q792L and D643G). Among the three additional mutations of XYNC, N536I was localized close to the active-site canyon on the protein surface, whereas the other two mutations (M564K and L833W) had side-chains localized in the protein's interior.

The sum effect of XYNA mutations (D592G, V632A, K789E, and I837M) was slightly stabilizing at 100 °C. D592G removed a negative charge from the middle of the negatively charged region on the protein surface, thus potentially reducing repulsive forces. V632 is part of a hydrophobic patch under an alpha-helix. The V632A mutation increased the helix propensity, thus potentially stabilizing the region. K789 is at the turning N-terminal end of a β-strand, and K789E forms a potential new H-bond between two β-strands. In mutation I837M, both Ile and Met filled a hydrophobic pocket, but Met led to a higher helix propensity, thus potentially stabilizing the region. It seems that the increased stability of alpha-helices and β-strands could underlie the effect of the mutations of the XYNA variant.

The new mutations of XYNB (N562D, T568M, R575G, D643G, and Q792L), with much-lowered thermostability, were analyzed in Swiss-PdbViewer (https://spdbv.unil.ch/) for their destabilization potential. N562 lines the active-site canyon and can form an H-bond with the substrate. N562D added a negative charge and, thus, formed a salt bridge with nearby Lys, possibly forming an H-bond with the substrate. This mutation could have affected the pH profile of the enzyme, but the destabilization effect was not clear. T568M formed H-bonding to the long Met side-chain over a cleft, positioned in a short helix belonging to a long loop structure.

Table 3 The binding free energies calculated by the MM-PBSA method.

Enzyme	ΔG_{gas} (kcal/mol)	ΔG_{gas} (kcal/mol)	ΔG (kcal/mol)
1VBR-X4-Phe806	-96.9695	73.6601	-23.3095
1VBR-X4-His806	-144.0604	106.2258	-37.8346
1VBR-X4-Ile806	-72.0392	65.9059	-6.1334
1VBR-X4-Leu806	-94.8851	68.1471	-26.7380
1VBR-X4-Val806	-116.1779	92.8110	-23.3669

$\Delta G = \Delta G_{gas} + \Delta G_{gas} - T\Delta S$; ΔG_{gas} and ΔG_{gas} represent the vacuum and solvation binding free energies, respectively. $-T\Delta S$ is the entropic contribution, which is not considered in the relative free energy analysis.

Met has higher helix propensity than Thr. For these reasons, the effect of the mutation was not clear. R575 forms a salt-bridge pair with the nearby E572 on the protein surface loop, and there is a hydrophobic interaction between the aliphatic parts of the side-chains. R575G removed the whole side chain, thus potentially destabilizing the loop structure.

D643 is localized in the protein's interior between two His side-chains, forming an H-bond to one of them. In this region, the charge of Asp seems to be neutralized by the His residues. D643G created a cavity inside the protein quite close to the catalytic residues (4.85 Å between carbonyl oxygens). The mutation may have also affected the pH profiles, and the created cavity and the removed H-bond may have negatively affected the thermostability. Q792 forms two H-bonds to two nearby side-chains in the protein's interior. Q792L removed them. Leu at position 792 formed a hydrophobic interaction with I557, thus partly compensating for the removed interaction but toward a different position. The net effect was potentially destabilizing.

The new mutations in XYNC were analyzed for their destabilization potential. The mutation N536I was localized in a turning loop on the C-terminal side of a barrel β-strand. Asn can form a H-bond in this partly hydrophobic surface pocket. Ile was surrounded by both hydrophobic and polar groups. Asn has stronger turn propensity than Ile. The effect of mutating Asn to Ile was not clear, but Asn is potentially more stabilizing in this position. M564K was localized in a long loop between a barrel helix and strand. The side-chain pointed into a tightly packed hydrophobic space between an α-helix and a β-sheet layer of a barrel, i.e., in the protein's interior. This region forms a highly hydrophobic pocket. Lys does not fully fit into this region and created a potential charge in a hydrophobic pocket inside the protein. In addition, the distance between the Lys NZ atom to the Val CG1 atom was only 2.6 Å. These findings suggest that the positively charged Lys side-chain was potentially creating destabilization in the hydrophobic protein interior (Denisov et al. 2004). Even if a change in the p*K*a of Lys would make it neutral, nevertheless, it is polar and too big to this space, and thus, it could be destabilizing. L833W was localized in the middle of an alpha-helix oriented toward two β-strands in the protein's interior. Leu resides in a full hydrophobic pocket inside the protein. Trp was too bulky for this space, clashing with neighboring hydrophobic side-chains; therefore, it is likely to be destabilizing.

The results obtained from mutagenesis experiments showed that the structure of extremophilic TmXYN10B still has several positions, at which mutations can improve its stability. On the other hand, as expected, many mutations were seemingly destabilizing by causing minor changes. The most destabilizing mutations likely involved introducing too large side-chains into the protein's interior, causing clashes and probably changing the structure. The structural stability of TmXYN10B is high enough to tolerate these kinds of changes in the XYNB variant, thus retaining the thermophilic nature of the enzyme with a T_m well above 70 °C. Therefore, its extreme stability allows the creation of such mutations via mutagenesis that may be useful but could compromise stability.

Hyperthermophilic α-amylases and a GH11 xylanase have been engineered to have in some degree higher stability at 100 °C (Li et al. 2013; Lim and Oslan 2021). When extreme stabilization is the goal of enzyme engineering, the mutations in TmXYN10B showed that also the thermostability of the most thermostable enzymes can be significantly improved by modifying even the active site. Hydrophobic interactions between the substrate and enzyme appear to play an important role in the enzyme's activity at extremely high temperatures. Since it is known that H-bonds become weaker and hydrophobic interactions become stronger at elevated temperatures, TmXYN10B relies on optimized hydrophobicity for its activity. Although the F806H mutant could form a stabilizing hydrogen bond to the substrate, the replacement of the apolar Phe with the polar His in a hydrophobic pocket at the edge of the active site improved the thermostability, even without the presence of the substrate. Furthermore, the molecular dynamics simulation with the substrate showed that the F806H variant had the highest deltaG, indicating a highest stability. However, the hydrophobic interaction between the substrate and the native Phe side-chain at position 806 contributed to the highest activity at extreme temperatures. Since the studied active site regions in different GH10 enzymes vary greatly in the amino acid composition, studying them more carefully is likely to give new insights how extremophilic enzymes optimize the flexibility and stability in the active site.

Supplementary Information The online version contains supplementary material available at https://doi.org/10.1007/s00253-022-11823-3.

Acknowledgements This work was financially supported by the project (no. DY135-B2-07) from the China Ocean Mineral Resources R&D Association, Hubei Provincial Technical Innovation Program (no. 2018ABA093).

Author contribution YW, OT, and HX conceived and designed research. YW, JW, and ZZ conducted experiments. JY and OT analyzed data. YW, OT, and HX wrote the manuscript. All authors read and approved the manuscript.

Data availability All data generated or analyzed during this study are included in this published article (and its supplementary information files).

Declarations

Ethics approval This article does not contain any studies with human participants or animals performed by any of the authors.

Conflict of interest The authors declare no competing interests.

References

Basit A, Liu J, Rahim K, Jiang W, Lou H (2018) Thermophilic xylanases: from bench to bottle. Crit Rev Biotechnol 38:989–1002

Bhalla A, Bansal N, Kumar S, Bischoff KM, Sani RK (2013) Improved lignocellulose conversion to biofuels with thermophilic bacteria and thermostable enzymes. Bioresour Technol 128:751–759

Bommarius AS, Paye MF (2013) Stabilizing biocatalysts. Chem Soc Rev 42:6534–6565

Camilloni C, Bonetti D, Morrone A, Giri R, Dobson CM, Brunori M, Gianni S, Vendruscolo M (2016) Towards a structural biology of the hydrophobic effect in protein folding. Sci Rep 6:28285

Chaudhary R, Kuthiala T, Singh G, Rarotra S, Kaur A, Arya SK, Kumar P (2021) Current status of xylanase for biofuel production: a review on classification and characterization. Biomass Conv Bioref. https://doi.org/10.1007/s13399-021-01948-2

Chawachart N, Anbarasan S, Turunen S, Li H, Khanongnuch C, Hummel M, Sixta H, Granstrom T, Lumyong S, Turunen O (2014) Thermal behaviour and tolerance to ionic liquid [emim]OAc in GH10 xylanase from *Thermoascus aurantiacus* SL16W. Extremophiles 18:1023–1034

Collins T, Gerday C, Feller G (2005) Xylanases, xylanase families and extremophilic xylanases. FEMS Microbiol Rev 29:3–23

Denisov VP, Schlessman JL, Garcia-Moreno EB, Halle B (2004) Stabilization of internal charges in a protein: water penetration or conformational change? Biophys J 87:3982–3994

Dougherty RC (1998) Temperature and pressure dependence of hydrogen bond strength: a perturbation molecular orbital approach. J Chem Phys 109:7372–7378

Dumon C, Varvak A, Wall MA, Flint JE, Lewis RJ, Lakey JH, Morland C, Luginbuhl P, Healey S, Todaro T, DeSantis G, Sun M, Parra-Gessert L, Tan X, Weiner DP, Gilbert HJ (2008) Engineering hyperthermostability into a GH11 xylanase is mediated by subtle changes to protein structure. J Biol Chem 283:22557–22564

Ericsson UB, Hallberg BM, Detitta GT, Dekker N, Nordlund P (2006) Thermofluor-based high-throughput stability optimization of proteins for structural studies. Anal Biochem 357:289–298

Gromiha MM, Pathak MC, Saraboji K, Ortlund EA, Gaucher EA (2013) Hydrophobic environment is a key factor for the stability of thermophilic proteins. Proteins 81:715–721

Hämäläinen J, Granström T, Mollerup F, Wang Y, Xiong H, Turunen O (2016) Effect of enzymatic high temperature prehydrolysis on the subsequent cellulose hydrolysis of steam-pretreated spruce in high solids concentration. J Chem Technol Biotechnol 91:1844–1852

Hebal H, Parviainen A, Anbarasan S, Li H, Makkonen L, Bankar S, King AWT, Kilpeläinen I, Benallaoua S, Turunen O (2020) Inhibition of hyperthermostable xylanases by superbase ionic liquids. Process Biochem 95:148–156

Hebal H, Boucherba N, Binay B, Turunen O (2021) Activity and stability of hyperthermostable cellulases and xylanases in ionic liquids. Biocatal Biotransformation 39:242–259

Ihsanawati KT, Kaneko T, Morokuma C, Yatsunami R, Sato T, Nakamura S, Tanaka N (2005) Structural basis of the substrate subsite and the highly thermal stability of xylanase 10B from *Thermotoga maritima* MSB8. Proteins 61:999–1009

Johnson RJ, Savas CJ, Kartje Z, Hoops GC (2014) Rapid and adaptable measurement of protein thermal stability by differential scanning fluorimetry: updating a common biochemical laboratory experiment. J Chem Educ 91:1077–1080

Kamerzell TJ, Middaugh CR (2008) The complex inter-relationships between protein flexibility and stability. J Pharm Sci 97:3494–3517

Kashif A, Tran LH, Jang SH, Lee CW (2017) Roles of active-site aromatic residues in cold adaptation of *Sphingomonas glacialis* esterase EstSP1. ACS Omega 2:8760–8769

Katewadee B, Penchit C, Pattanop K, Verawat C (2021) Enhancement of catalytic performance of a metagenome-derived thermophilic oligosaccharide-specific xylanase by binding module removal and random mutagenesis. J Biosci Bioeng 131:13–19

Kumar V, Dangi AK, Shukla P (2018) Engineering thermostable microbial xylanases toward its industrial applications. Mol Biotechnol 60:226–235

Lai Z, Zhou C, Ma X, Xue Y, Ma Y (2021) Enzymatic characterization of a novel thermostable and alkaline tolerant GH10 xylanase and activity improvement by multiple rational mutagenesis strategies. Int J Biol Macromol 170:164–177

Li H, Kankaanpää A, Xiong H, Hummel M, Sixta H, Ojamo H, Turunen O (2013) Thermostabilization of extremophilic *Dictyoglomus thermophilum* GH11 xylanase by an N-terminal disulfide bridge and the effect of ionic liquid [emim]OAc on the enzymatic performance. Enzym Microb Technol 53:414–419

Li G, Fang X, Su F, Chen Y, Xu L, Yan Y (2018) Enhancing the thermostability of *Rhizomucor miehei* lipase with a limited screening library by rational-design point mutations and disulfide bonds. Appl Environ Microbiol 84:e02129–e02117

Li G, Zhou X, Li Z, Liu Y, Liu D, Miao Y, Wan Q, Zhang R (2021) Significantly improving the thermostability of a hyperthermophilic GH10 family xylanase XynAF1 by semi-rational design. Appl Microbiol Biotechnol 105:4561–4576

Lim SJ, Oslan SN (2021) Native to designed: microbial α-amylases for industrial applications. PeerJ 9:e11315

Miyazaki K, Takenouchi M, Kondo H, Noro N, Suzuki M, Tsuda S (2006) Thermal stabilization of *Bacillus subtilis* family-11 xylanase by directed evolution. J Biol Chem 281:10236–10242

Nakamura A, Tsukada T, Auer S, Furuta T, Wada M, Koivula A, Igarashi K, Samejima M (2013) The tryptophan residue at the active site tunnel entrance of *Trichoderma reesei* cellobiohydrolase Cel7A is important for initiation of degradation of crystalline cellulose. J Biol Chem 288:13503–13510

Prajapati AS, Pawar VA, Panchal KJ, Sudhir AP, Dave BR, Patel DH, Subramanian RB (2018) Effects of substrate binding site residue substitutions of xynA from *Bacillus amyloliquefaciens* on substrate specificity. BMC Biotechnol 18:9

Shoichet BK, Baase WA, Kuroki R, Matthews BW (1995) A relationship between protein stability and protein function. Proc Natl Acad Sci U S A 92:452–456

Simpson HD, Haufler UR, Daniel RM (1991) An extremely thermostable xylanase from the thermophilic eubacterium *Thermotoga*. Biochem J 277:413–417

Song L, Tsang A, Sylvestre M (2015) Engineering a thermostable fungal GH10 xylanase, importance of N-terminal amino acids. Biotechnol Bioeng 112:1081–1091

Taylor MP, Eley KL, Martin S, Tuffin M, Burton SG, Cowan DA (2009) Thermophilic ethanologenesis: future prospects for second-generation bioethanol production. Trends Biotechnol 27:398–405

Tian L, Liu S, Wang S, Wang L (2016) Ligand-binding specificity and promiscuity of the main lignocellulolytic enzyme families as revealed by active-site architecture analysis. Sci Rep 6:23605

Torktaz I, Karkhane AA, Hemmat J (2018) Rational engineering of Cel5E from *Clostridium thermocellum* to improve its thermal stability and catalytic activity. Appl Microbiol Biotechnol 102:8389–8402

Tu T, Luo H, Meng K, Cheng Y, Ma R, Shi P, Huang H, Bai Y, Wang Y, Zhang L, Yao B (2015) Improvement in thermostability of an *Achaetomium* sp. strain Xz8 endopolygalacturonase via the

optimization of charge-charge interactions. Appl Environ Microbiol 81:6938–6944

Tu T, Li Y, Luo Y, Wang Z, Wang Y, Luo H, Yao B (2018) A key residue for the substrate affinity enhancement of a thermophilic endo-polygalacturonase revealed by computational design. Appl Microbiol Biotechnol 102:4457–4466

Turunen O, Jänis J, Fenel F, Leisola M (2004) Engineering the thermotolerance and pH optimum of family 11 xylanases by site-directed mutagenesis. Methods Enzymol 388:156–167

van Dijk E, Hoogeveen A, Abeln S (2015) The hydrophobic temperature dependence of amino acids directly calculated from protein structures. PLoS Comput Biol 11:e1004277

Wang Y, Fu Z, Huang H, Zhang H, Yao B, Xiong H, Turunen O (2012) Improved thermal performance of *Thermomyces lanuginosus* GH-11 xylanase by engineering of an N-terminal disulfide bridge. Bioresour Technol 112:275–279

Wang K, Luo H, Tian J, Turunen O, Huang H, Shi P, Hua H, Wang C, Wang S, Yao B (2014) Thermostablility improvement of a *Streptomyces* xylanase by introducing proline and glutamic acid residues. Appl Environ Microbiol 80:2158–2165

Wang Y, Bai Y, Shu T, Fan P, Zhang H, Turunen O, Xiong H, Yu L (2020) Characterization of a versatile glycoside hydrolase Cel5M from *Pectobacterium carotovorum* HG-49 for ramie degumming. Text Res J 90:1602–1615

Winterhalter C, Liebl W (1995) Two extremely thermostable xylanases of the hyperthermophilic bacterium *Thermotoga maritima* MSB8. Appl Environ Microbiol 61:1810–1815

Wu Z, Zhao C, Huang Y, Ye F, Zhao G (2020) Molecular mechanism underlying the effects of temperature and pH on the size and surface charge of octenylsuccinated oat β-glucan aggregates. Carbohydr Polym 237:116115

Yang J, Han Z (2018) Understanding the positional binding and substrate interaction of a highly thermostable GH10 xylanase from *Thermotoga maritima* by molecular docking. Biomolecules 8:64

Yang J, Ma T, Shang-guan F, Han Z (2020) Improving the catalytic activity of thermostable xylanase from *Thermotoga maritima* via mutagenesis of non-catalytic residues at glycone subsites. Enzym Microb Technol 139:109579

Yi Y, Xu S, Kovalevsky A, Zhang X, Liu D, Wan Q (2021) Characterization and structural analysis of a thermophilic GH11 xylanase from compost metatranscriptome. Appl Microbiol Biotechnol 105:7757–7767

You C, Huang Q, Xue H, Xu Y, Lu H (2010) Potential hydrophobic interaction between two cysteines in interior hydrophobic region improves thermostability of a family 11 xylanase from *Neocallimastix patriciarum*. Biotechnol Bioeng 105:861–870

Yu T, Anbarasan S, Wang Y, Telli K, Aslan AS, Su Z, Zhou Y, Zhang L, Iivonen P, Havukainen S, Mentunen T, Hummel M, Sixta H, Binay B, Turunen O, Xiong H (2016) Hyperthermostable *Thermotoga maritima* xylanase XYN10B shows high activity at high temperatures in the presence of biomass-dissolving hydrophilic ionic liquids. Extremophiles 20:515–524